IETE Journal of Research

ISSN: 0377-2063 (Print) 0974-780X (Online) Journal homepage: www.tandfonline.com/journals/tijr20

An Approach for Diagnostically Lossless Coding of Volumetric Medical Data Based on Wavelet and Just-Noticeable-Distortion Model

B. K. Chandrika, P. Aparna & S. Sumam David

To cite this article: B. K. Chandrika, P. Aparna & S. Sumam David (2023) An Approach for Diagnostically Lossless Coding of Volumetric Medical Data Based on Wavelet and Just-Noticeable-Distortion Model, IETE Journal of Research, 69:2, 896-908, DOI: 10.1080/03772063.2020.1844070

To link to this article: https://doi.org/10.1080/03772063.2020.1844070

Published online: 16 Nov 2020.

IETE JOURNAL OF RESEARCH
2023, VOL. 69, NO. 2, 896–908
https://doi.org/10.1080/03772063.2020.1844070

An Approach for Diagnostically Lossless Coding of Volumetric Medical Data Based on Wavelet and Just-Noticeable-Distortion Model

B. K. Chandrika [1], P. Aparna [2] and S. Sumam David [2]

[1]Manipal Institute of Technology, Manipal Academy of Higher Education, Manipal, India, 576 104; [2]Department of Electronics & Communication Engineering, National Institute of Technology Karnataka, Surathkal, India, 575 025

ABSTRACT

This paper explores a technique for visually/diagnostically lossless coding in the wavelet domain to effectively compress the three-dimensional medical image data. The quantisation module based on Just Noticeable Distortion (JND) for wavelets guarantees the visual quality in the reconstructed data. This method has been further extended to present the Volume of Interest (VOI) based technique that enables to preserve the quality of the diagnostically significant VOI region. The proposed method tested on several datasets outperforms the state-of-the-art methods. Apart from the conventional quality metric, Human Visual System (HVS) based quality metrics are also used to evaluate the visual quality of the reconstructed image. A subjective and objective evaluation carried out for VOI based coder shows that the quality-compression needs of the medical community are well addressed.

KEYWORDS

Discrete wavelet transform; Just noticeable distortion; Medical image coding; MRI and CT images; Visually lossless compression; Volume of interest

1. INTRODUCTION

Modern medical imaging modalities such as Computed Tomography (CT), Positron Emission Tomography (PET), Ultrasound, Magnetic Resonance Imaging (MRI), *etc*., have revolutionised the health care systems. Improved inter-slice distance, increased image resolution, and medical image data volume plays a significant role in early intervention and detailed diagnosis of health condition resulting in substantial image data. Hence, the paramount problem is to manage this enormous amount of data for storage and transmission. Medical diagnostic techniques for detection of abnormalities demand high visual quality in the image, which is possible with lossless compression. But these lossless compression techniques offer poor compression that can't meet the current compression requirements.

On the other hand, lossy techniques offer good compression but with a quality unacceptable to the medical community. Hence, the need of the hour is to achieve better compression than lossless methods with quality much better than that of lossy techniques acceptable to the medical community. Compression technique based on HVS is an ideal way to achieve this. These methods eliminate visually redundant data without altering any data of diagnostic significance.

In this context, a brief literature survey on various compression techniques available for medical image data is presented. Compression algorithms used to compress medical images in the early 1990s assumed that there is no correlation among adjacent image slices and hence compressed each image slice independently without exploiting inter-slice correlation. Compression algorithms used for still images were modified, or new algorithms were developed to exploit inter-slice correlation [1–3] to improve the compression ratio. Telemedicine applications demand scalability in the compression algorithm, to support lossy-to-lossless compression framework. This framework would enable the physicians to examine the lower bit rate version in the first stage. However, if any abnormality is detected, more bits can be requested to enhance the quality. This flexibility can be well addressed by wavelet transform because of its inherent scalability.

Wavelet based compression in [4–9] independently decodes 2D medical images of diagnostic importance, without reconstructing the entire image volume. Integer wavelet transform based algorithm presented by [4] for 3D medical image compression use Embedded Zero Wavelet (EZW) scheme with context based arithmetic coding. Menegaz *et al.* [5] developed a fully 3D object based coding technique to independently decode different objects based on diagnostic relevance in volumetric data. They decorrelated the input data with 3D Discrete Wavelet Transform (DWT), providing a provision for lossless coding. Also, Menegaz *et al.* [6] developed a

3D wavelet based coding method to enable 3D encoding and 2D decoding functionality. Zixiang Xiong *et al.* applied a technique that provides an option of lossy or lossless decoding on 3D medical data [7]. Few of the region/volume based medical image compression techniques are [10–13]. The 3D medical image compression method proposed by Sanchez *et al.* [14] has the scalability feature and also considers Volume of Interest (VOI) based coding for interactive telemedicine applications. This particular compression technique provides random access of VOI with a provision for quality and resolution scalability, hence providing the ability to decode any section of the compressed image without decoding the entire data set. These features were achieved with Embedded Block Coding with Optimized Truncation (EBCOT) embedded in 3D integer wavelet transform to generate a scalable layered bit stream. Resolution scalability is a desired feature in the compression of medical images. 3D Discrete Cosine Transform (DCT) fails to offer a quality of lossless coding and resolution scalability. Jonathan Taquet *et al.* [15] proposed a lossless and near-lossless compression technique based on a modified hierarchical approach. The resolution scalability is achieved by combining Differential Pulse Code Modulation (DPCM) schemes with modified hierarchical based predictors. Sanchez *et al.* [16] proposed High Efficiency Video Coding (HEVC) based intra coding for reversible compression of 3D medical images. Bruylants *et al.* [17] presented a wavelet based volumetric medical image compression algorithm, which supports the volumetric extension of Joint Photographic Experts Group (JPEG) 2000 standard.

An alternative to lossless and lossy compression schemes is visually lossless image coding. Compression performance in visually lossless algorithms is better than reversible coding schemes while maintaining the reconstructed image quality within the human perception. That is, it permits greater compression gain through the removal of visually redundant information without inducing any perceptible distortions. David Wu *et al.* [18] proposed a simple perceptual based compression algorithm to compress 2D MRI, Computed Radiography, and CT medical image data sets. The visual pruning scheme developed is based on the JPEG 2000 compression structure. The vision model is merged with an improved HVS model to identify and estimate visually redundant information.

This paper proposes a diagnostically/visually lossless compression approach for MRI and CT sequences. The significant contributions of this work are as follows:

(i) Our method embeds a wavelet based vision model to remove visually redundant information. This scheme utilises a distortion metric based on human perception that exploits contrast and luminance masking properties of the HVS.
(ii) Block matching technique is employed to eliminate inter-slice redundancy across the slices.
(iii) The proposed wavelet based technique is further extended to develop VOI based compression, which uses symmetry based tumour segmentation algorithm to identify the diagnostically important region.
(iv) HVS based quality metrics are applied to estimate the quality of the compression algorithm and has been cross verified by the medical experts.

The proposed work has been extensively compared with the state-of-the-art lossless coders in terms of compression performance and with lossy coders for rate distortion performance. The proposed compression techniques are described in detail in Section 2 and Section 3. In Section 4, medical data sequences used to test the algorithms are introduced. Section 5 reports on experimental results and presents a discussion on the performance of the proposed method. Section 6 derives conclusions.

2. PROPOSED WAVELET BASED CODING METHOD

Wavelet based compression supports resolution scalability and lossy-to-lossless coding framework. The block diagram of the proposed wavelet based Visually Lossless Image Compression (VLIC) technique for volumetric medical data is illustrated in Figure 1. Each slice is first decomposed up to n levels with DWT. A wavelet based vision model is used to measure the JND followed by a JND dependent quantizer to remove visually irrelevant information. On the resulting image slices, the block matching algorithm is applied to remove inter-slice redundancy. The image residue and displacement vectors generated by the block matching algorithm are compressed using arithmetic coding. A wavelet based vision model based on mixed masking effects of HVS is used in our coding technique to determine Just Noticeable Distortion (JND) threshold. Wavelet based distortion threshold value changes with the orientation, local frequency, and spatial features of the visual information such as contrast and luminance masking. Obtained threshold values are used to retain the perceptual quality of the image by eliminating only visually redundant information.

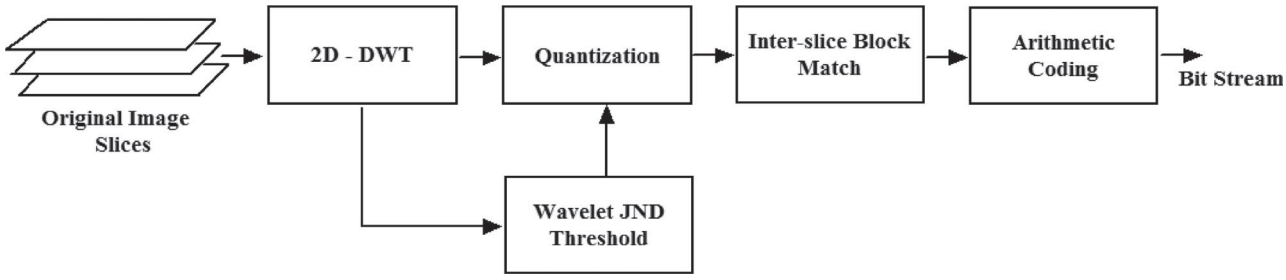

Figure 1: Block diagram of the proposed visually lossless compression technique.

2.1 JND Thresholds for Wavelet Coefficient

The function of JND profile is to measure the perceptual redundancy present in an image. The visual model uses one JND threshold value, $v_{\mathrm{JND}}(h,\phi,[l,m])$ for every DWT coefficient at position $[l,m]$ in subband (h,ϕ) where h is the decomposition level, and ϕ is the orientation. The important visual characteristics considered in this work are luminance masking or light adaption, contrast sensitivity, and contrast masking to determine the JND threshold [19]. The JND threshold is thus computed as:

$$v_{\mathrm{JND}}(h,\phi,[l,m]) = \mathrm{JND}_{(h,\phi)}\, a_{la}(h,\phi,[l,m])\, a_c(h,\phi,[l,m]) \quad (1)$$

where $\mathrm{JND}_{(h,\phi)}$ is the base detection threshold of a subband (h,ϕ), $a_{la}(h,\phi,[l,m])$ is the light adaptation correction and $a_c(h,\phi,[l,m])$ is the contrast masking correction. The base detection threshold $\mathrm{JND}_{(h,\phi)}$ for each subband (h,ϕ) provides the relative change in the visible light over a background with uniform intensity.

The expression for $\mathrm{JND}_{(h,\phi)}$ is specified as [19]:

$$\mathrm{JND}_{(h,\phi)} = \frac{a10^{p\left\{\log\left(\frac{g_\phi f 2^h}{r}\right)\right\}^2}}{A_{(h,\phi)}} \quad (2)$$

where a, p, f, r, and g_ϕ are constants. $A_{(h,\phi)}$ is the magnitude of the DWT 9/7 kernel basis function [19]. Its value depends on visual resolution of the display in pixels/degree r, decomposition level h, and orientation ϕ.

The variation in the background intensity alters the base detection threshold value. Hence, there is a need for considering the mean luminance of the local image region when calculating detection threshold. So, another compensating factor luminance masking is added to the contrast sensitivity basis function. The luminance masking adaptation factor is estimated as:

$$a_{la}(h,\phi,[l,m]) = \left(\frac{c(h_{\max},LL,[l',m'])}{c_{\mathrm{mean}}}\right)^{a_T} \quad (3)$$

where $c(h_{\max},LL,[l',m'])$ is the value of the DWT coefficient in the LL subband that spatially corresponds to the position $(h,\phi,[l,m])$. In this case, l' and m' can be calculated as $l' = \left\lfloor \frac{l}{2^{(h_{\max}-h)}} \right\rfloor$ and $m' = \left\lfloor \frac{m}{2^{(h_{\max}-h)}} \right\rfloor$. The parameter a_T controls luminance masking and a value of 0.649 was used [19]. The presence of an image component can alter the visibility of the other image component [19]. To address this, contrast masking is used, and hence the variation in the detection threshold of a target signal is varied as a function of contrast masking. The contrast masking effect has two components and is evaluated as:

$$a_c(h,\phi,[l,m]) = a_{c\_\mathrm{self}}(h,\phi,[l,m])\, a_{c\_\mathrm{neigh}}(h,\phi,[l,m]) \quad (4)$$

where $a_{c\_\mathrm{self}}(h,\phi,[l,m])$ is the self-contrast masking correction factor and $a_{c\_\mathrm{neigh}}(h,\phi,[l,m])$ is the neighbourhood contrast masking correction factor.

A sufficiently large DWT coefficient at the location $(h,\phi,[l,m])$ raises the detection threshold. So, in this work, the effect of variation in detection threshold is taken into account through a self-contrast masking correction factor $a_{c\_\mathrm{self}}(h,\phi,[l,m])$. For the DWT coefficients, it is expressed as:

$$a_{c\_\mathrm{self}}(h,\phi,[l,m]) = \max\left\{1, \left(\frac{|c(h,\phi,[l,m])|}{\mathrm{JND}_{(h,\phi)}\, a_{la}(h,\phi,[l,m])}\right)^{\epsilon}\right\} \quad (5)$$

where $c(h,\phi,[l,m])$ is the DWT coefficient value at location $(h,\phi,[l,m])$. For the lowest subband, contrast masking is not applied ($\epsilon = 0$). For other subbands, ϵ is 0.6 [19].

In the case of wavelet based reconstructed images, the pixel value framed by wavelet coefficient $c(h,\phi,[l,m])$ is overlapped on other pixel values framed by the spatially neighbouring wavelet coefficients. So there is a kind of masking effect contributed from spatially neighbouring signals in wavelet domain [19]. To account for this

phenomena neighbourhood contrast correction factor $a_{c\_\text{neigh}}(h, \phi, [l, m])$ is incorporated.

It is expressed as:

$$a_{c\_\text{neigh}}(h, \phi, [l, m]) = \max \left\{ 1, \sum_{k \in \text{neighbours of } (h,\phi,[l,m])} \times \frac{\left| \frac{c_k}{\text{JND}_{(h,\phi)} a_{la}(h,\phi,[l,m])} \right|^{\xi}}{N_{[l,m]}} \right\} \quad (6)$$

where the spatial neighbourhood considered contains the DWT coefficients belonging to the same subband that lie within a window centred at the position $[l, m]$. $N_{[l,m]}$ represents the number of coefficients in that neighbourhood. c_k is the neighbouring wavelet transform coefficient. $\xi = 0.5$ is a constant that regulates the impact of the value of each neighbouring coefficient.

2.2 JND Dependent Quantizer

The simplest approach for eliminating the visually redundant information from DWT coefficients is to quantise the DWT coefficients in such a manner that the absolute value of quantisation error is below the JND value. After determining JND value for each wavelet coefficients, the reference or original DWT coefficient $c(h, \phi, [l, m])$ is quantised to get $cd_k(h, \phi, [l, m])$ through truncation of $c(h, \phi, [l, m])$. So

$$cd_k(h, \phi, [l, m]) = \left\lfloor \frac{c(h, \phi, [l, m])}{k} \right\rfloor \times k \quad (7)$$

where $\lfloor \rfloor$ is the truncation function and k is an integer. Eventually, if the quantised DWT coefficient $cd_k(h, \phi, [l, m])$ is below the JND threshold $v_{\text{JND}}(h, \phi, [l, m])$, the DWT coefficient $c(h, \phi, [l, m])$ at location $[l, m]$ is replaced by the corresponding quantised DWT coefficient $cd_k(h, \phi, [l, m])$.

2.3 Inter-Slice Block Matching

Each slice is transection of the human body. The inter-slice distance typically in the range of 0.5 mm to 5 mm. So, there exists a lot of structural similarity between the successive slices.

In this stage, compression can be further improved by removing the redundancy across these slices. Inter-slice block match algorithm is used to determine the residual of the current slice with previous image slice as a reference. The residual image so obtained is further encoded using adaptive arithmetic coding.

2.4 Arithmetic Coding

Arithmetic coding is one of the entropy coding methods used to remove statistical redundancies in the image. Residual image and displacement vectors obtained from block matching routine are encoded with context adaptive binary arithmetic coder.

3. EXTENSION OF WAVELET BASED TECHNIQUE TO VOI METHOD

In most of the cases, all the image slices acquired, or the entire region of medical images may not be required for further investigation. So once the abnormality is detected in a particular region across all slices, apply a technique that preserves the quality of diagnostically significant VOI. In this context, the VOI based compression technique for MRI brain images is proposed, as shown in Figure 2. This algorithm identifies the ROI/VOI and applies a visually lossless compression technique to this region, while the other part is compressed with a lossy technique. Symmetry based tumour segmentation algorithm is used to detect the diagnostically relevant region in each image slice, and hence, VOI is determined across all image slices. Wavelet based VLIC is applied on the segmented VOI, and DCT based lossy compression technique is applied to the residual image.

3.1 Symmetry Based Bounding Box Segmentation for Tumour Detection

An automatic segmentation method based on symmetry is used to identify the ROI. Initially, the line of symmetry is obtained by computing a gradient vector flow snake to find the skull boundary [20]. The vertical line passing through the centroid of the snake is considered as the axis of symmetry. Each MRI brain image slice is split along the line of symmetry into two halves. One half of the image is viewed as the reference image R and the other half as the test image T. Thus, the assumption made is that abnormality is located either in the reference or in the test image. Next, the image T is compared with image R to locate the deceased area. Point wise subtraction is the straight forward method used to compare two images. But many times, point wise subtraction of images $T - R$ fails to recognise the region of an abnormality since the symmetry across two halves of a brain is not perfect. So region based segmentation method is used. In this segmentation technique, a score function interpreted by the Bhattacharya coefficient is used [21]. Image intensity histograms of T and R are used to detect the abnormality.

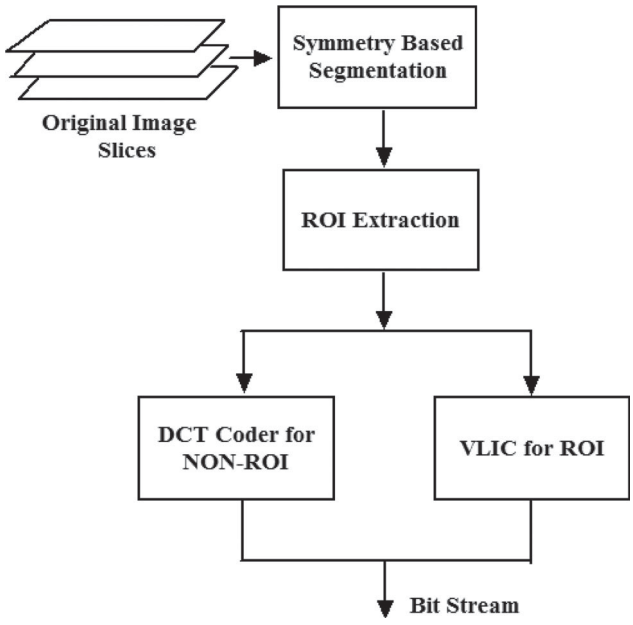

Figure 2: VOI based coder.

3.2 Wavelet Based Visually Lossless Compression

The diagnostically important region in each image slice is obtained with symmetry based bounding box segmentation algorithm. The ROI in each of the slices grouped to form VOI. Wavelet based VLIC explained in Section 2 is used to compress image within VOI.

3.3 DCT Based Lossy Compression

The region outside the VOI is compressed using DCT based lossy compression technique. Image outside the ROI is divided into non-overlapping spatial blocks of size 8×8. Every block is transformed from the pixel domain to the frequency domain using 2-D DCT. In the DCT domain information is concentrated among few coefficients and hence can be easily compressed.

3.4 Quantisation

The DCT coefficients are quantised using scalar quantisation. Each of the DCT coefficients is divided by its corresponding quantizer, followed by rounding to its nearest integer [22]. This is given by

$$I_q(x,y) = \text{Integer Round}\left[\frac{I(x,y)}{Q(x,y)}\right] \tag{8}$$

where $I(x,y)$ represents the transformed coefficient, $I_q(x,y)$ represents the quantised coefficient, $Q(x,y)$ represents the quantizer value. In principle, these values can be specified and fine-tuned by the user for maximum compression or quality. In this work, the quantizer value chosen is from a JPEG standard [22]. After applying wavelet based VLIC for images within VOI and DCT based lossy technique to images outside VOI, a simple prediction method is applied to exploit slice redundancy. The predicted quantised transform domain coefficients are obtained by the following equation.

$$I_{qkr} = I_{qk} - I_{q(k-1)} \tag{9}$$

where I_{qkr} is the predicted k^{th} slice, I_{qk} is the quantised transform domain coefficient in k^{th} slice and $I_{q(k-1)}$ is the quantised transform domain coefficient in $(k-1)^{th}$ slice. Finally, predicted coefficients are encoded using context adaptive binary arithmetic coder.

4. DATA SET USED FOR TESTING THE COMPRESSION SCHEMES

The database used is 8 bit and 12 bit MRI, CT, and Angio sequences. Simulations were performed on more than 5000 slices of CT, 2000 slices of MRI, and around 600 slices of X-ray Angio images. Results obtained with 3157 slices of CT images, 886 slices of MR images, 608 slices of X-ray Angio slice, and 587 slices of MRI brain images with tumour are documented. Data set-1 consists of 8 bit images from Image Processing Lab, Mallinckrodt Institute of Radiology [4]. The second data set includes of 608 slices of 12 bit X-ray Angio images, 1315 slices of 12 bit CT images, and 8 bit 160 slices of MRI [16]. Volumes 1–3 are X-ray images of a vascular study of a human heart. Volumes 4–6 are axial view CT scan images of the human thorax. Volume 7 is axial view MRI scan of the human brain and volumes 8–9 are the sagittal view of MRI scan of the human spinal cord and knee. The third medical image data set consists of 12 bit images generated with CT and MRI scanners [17]. This data set has 1334 CT image slices and 550 MRI slices. Fourth test data set consists of volumes of 12 bit T1 and T2 weighted volumetric MRI brain images with tumour obtained from 1.5 Tesla MRI scanner from Hubli Scanning Center, Hubli, India. Details of all the three data sets mentioned are summarised in Table 1.

5. RESULTS AND DISCUSSIONS

The proposed methods have been simulated using Matlab® on an Intel® i7 Core processor. We tested wavelet based VLIC on 8 bit and 12 bit volumetric data sets used in [4,16,17] for comparison. However, the VOI based technique is tested on MRI brain sequences with tumour obtained from the diagnostic centre.

Table 1: Details of Medical Image Data sets.

Label	Bit per pixel	Number of slices	Resolution
Data set – 1 [4]			
CT Skull	8	192	256 × 256
CT Wrist	8	176	256 × 256
CT Carotid	8	64	256 × 256
CT Aperts	8	96	256 × 256
MRI Liver T1	8	48	256 × 256
MRI Liver T2	8	48	256 × 256
MRI Sag head	8	16	256 × 256
MRI Ped chest	8	64	256 × 256
Data set – 2 [16]			
X-ray Angio-1	12	151	512 × 512
X-ray Angio-2	12	271	512 × 512
X-ray Angio-3	12	186	512 × 512
CT-1 Human Thorax	12	596	512 × 512
CT-2 Human Thorax	12	637	512 × 512
CT-3 Human Thorax	12	82	512 × 512
MRI Brain	8	100	256 × 256
MRI Cord	8	10	512 × 512
MRI Knee	8	50	512 × 512
Data set – 3 [17]			
CT-4 Lung scan	12	201	512 × 512
CT-5 Lung scan	12	242	512 × 512
CT-6 Spiral Arterial scan	12	75	512 × 512
CT-7 Female cadaver	12	100	512 × 512
CT-8 Human cadave	12	672	512 × 512
CT-9 Chest	12	44	512 × 512
MRI-1 Brain	12	250	432 × 432
MRI-2 Brain	12	200	256 × 256
MRI-3 Brain	12	100	256 × 256
Data set – 4 (MRI brain images)			
Volume-1	12	100	256 × 176
Volume-2	12	18	512 × 304
Volume-3	12	18	512 × 304
Volume-4	12	30	512 × 336
Volume-5	12	18	512 × 304

5.1 Metrics for Evaluating Compression Algorithms

Both objective and subjective metrics are used to evaluate lossy compression algorithms. Peak Signal to Noise Ratio (PSNR) is the widely used quality metric to assess the lossy compression algorithms, even though all the time, it does correspond to subjective quality perceived by the HVS. Visual Information Fidelity (VIF) [23], Structural SIMilarity index (SSIM) [24–26] and Visual Signal to Noise Ratio (VSNR) [27] are some of the widely used HVS based objective metrics found in the literature. The proposed compression techniques use these metrics to estimate the perceptible grade of the reconstructed image.

VIF index is based on nonstructural distortions between two images. Components considered in the calculation of VIF quality metric are correlation distortion, luminance distortion, and contrast distortion. VIF quality estimation has two stages. First, information that can be gathered from the original image is computed. Loss of the same information in the processed (distorted) image is measured later. VIF between two images $a(x, y)$ and $b(x, y)$ is given by

$$\mathrm{VIF}(a, b) = \frac{\text{Distorted image information}}{\text{Reference image information}} \tag{10}$$

The value of VIF between the original image and its duplicate is 1.

SSIM index is based on the structural dependency among neighbouring pixels. SSIM metric estimates the similarity or difference between two images. SSIM index is based on brightness, contrast, and structure, which are the significant components of the HVS model. SSIM value between two images a and b is expressed as [24]:

$$\mathrm{SSIM}(a, b) = I(a, b)c(a, b)s(a, b) \tag{11}$$

where $I(a, b)$ is the luminance component, $c(a, b)$ is the contrast component and $s(a, b)$ is the structural component. So

$$I(a, b) = \left(\frac{2\sigma_a\sigma_b + \mathrm{C}_1}{{\sigma_a}^2 + {\sigma_b}^2 + \mathrm{C}_1}\right) \tag{12}$$

$$c(a, b) = \left(\frac{2\sigma_a\sigma_b}{{\sigma_a}^2 + {\sigma_b}^2 + C_2}\right) \tag{13}$$

$$s(a, b) = \left(\frac{\sigma_{ab} + 0.5C_2}{\sigma_a\sigma_b + 0.5C_2}\right) \tag{14}$$

where σ_a, σ_b is the average intensity of image a and b, respectively, ${\sigma_a}^2$ and ${\sigma_b}^2$ is the variance of image a and b, respectively, and σ_{ab} is the covariance.

SSIM is considered to be a measure of image quality close to that of subjective quality [28]. When two images a and b are exactly the same, value of $\mathrm{SSIM}(a, b) = 1$, and hence SSIM value close to 1 is desirable.

VSNR value calculation involves two stages. Image distortion is determined in the first stage. In this stage, the visibility of distortion in the reconstructed image is checked after computing the contrast detection threshold. If the distortions are below the threshold of detection, the reconstructed image is of perfect visual quality. If the distortions are above the threshold, the perceived contrast of the distortions d_{ac} and disruption of global precedence d_{ba} are computed to determine VSNR. VSNR between two images a and b is defined as:

$$\mathrm{VSNR}(a, b) = 20\log_{10}\left(\frac{C(a)}{\alpha d_{ac} + (1 - \alpha)\frac{d_{ba}}{\sqrt{2}}}\right) \tag{15}$$

where $C(a)$ is the contrast of the original image a, $d_{ac} = C(E)$ is the perceived contrast of the distortions, $E = a -$

Table 2: Bit rate and quality metrics of the reconstructed image with and without neighbourhood masking for data set-1 of Table 1.

	Self-masking				Self and neighbourhood masking			
Label	bpp	PSNR (dB)	VSNR (dB)	VIF	bpp	PSNR (dB)	VSNR (dB)	VIF
CT Skull	1.541	50.84	45.52	0.944	1.421	50.77	45.68	0.944
CT Wrist	0.808	52.58	52.73	0.942	0.736	52.54	52.76	0.942
CT Carotid	1.161	52.36	49.95	0.96	1.124	52.34	49.95	0.96
CT Aperts	0.716	54.95	56.31	0.958	0.661	54.92	56.34	0.958
MRI Liver T1	1.388	49.67	45.39	0.95	1.291	49.63	45.38	0.938
MRI Liver T2	1.209	51.83	46.35	0.959	1.177	51.82	46.33	0.957
MRI Sag head	1.439	51.15	52.71	0.92	1.285	51.11	52.75	0.927
MRI Ped chest	1.122	50.04	55.61	0.912	0.958	49.95	55.65	0.912

b is the distortion, d_{ba} is the global precedence and $\alpha \in [0, 1]$ determines the relative contribution of d_{ac} and d_{ba}.

In the subjective evaluation, radiologist review a series of compressed images which are diagnostically significant. For each image, a confidence rating is given based on the information provided by the compressed image for their impression on the possibility of the presence of the disease. Although this procedure is time consuming and tedious, it is a trusted and accepted method to certify the image quality.

5.2 Wavelet Based VLIC Technique

DWT is implemented with a 9/7 wavelet filter with five levels of scaling. The value of parameters a, p, f, r, and g_ϕ used in the JND model are based on the experiments carried with various models to express the threshold for grey scale DWT noise as a function of orientation ϕ and spatial frequency [29].

5.2.1 Impact of Neighbourhood Masking on Performance

The influence of considering neighbourhood contrast correction along with self-contrast correction with different bit rates as discussed in Section 2.1 is tested, and results are tabulated in Table 2. Table 2 compares quality metrics such as PSNR, VSNR, and VIF against the bit rate for VLIC, considering only self-masking and VLIC considering both self and neighbourhood masking. For almost the same quality, VLIC with both maskings gives a reduced bit rate. An overall improvement of 7.89 % is seen in bit rate. So both self and neighbourhood masking factors are considered in the implementation of the coder.

5.2.2 Effect of Decomposition Levels in DWT

It is important to check the effect of decomposition levels in DWT on visually lossless CR. As mentioned in Section 2.1, basis function amplitude $A_{(h,\phi)}$ is not the same for different frequency levels of DWT and hence the JND values. Hence, it is possible to represent the data in a more redundant form by increasing the number of levels of decomposition in DWT. Simulations were carried out for six levels of frequency decomposition with biorthogonal 9/7 wavelet filter set. As seen from Table 3, decomposing up to level-5 reduces bit rate for a small reduction in quality. However, there is only a marginal improvement in CR from level-5 to level-6. Considering all images in data set-1, the average reduction in bit rate from level-1 to level-5 is 35.46 %. Table 3 compares the bit rate (bpp) and corresponding PSNR(dB), VIF, and VSNR (dB) across the different levels. Tabulated PSNR, VIF, and VSNR values for levels 1–6 demonstrate that there is no perceivable distortion by increasing the decomposition levels since there is not much difference in quality metric values from decomposition level 1–6.

5.3 Rate-Distortion Performance

PSNR and HVS based quality assessment metrics like VIF, SSIM, and VSNR are computed and tabulated for VLIC and VOI methods at a particular bit rate, as shown in Table 4. Figure 3(a) shows an original image slice of CT Skull from dataset-1, while Figure 3(b) shows the reconstructed slice using VLIC method at a bit rate of 1.89 bpp and PSNR of 51.22 dB. For VOI based schemes region-A specifies the region of interest and region-B specifies a non-VOI region. The bit rate specified for VOI method is the average bit rate for both the regions. Figure 4(a) shows a coronal view of original MRI brain image slice from dataset-4, while Figure 4(b) shows the reconstructed slice using VOI method at an average bit rate of 2.022 bpp and PSNR of 75.27 dB for region-A and 60.88 dB for region-B. Figure 3, Figure 4, Figure 5, and Figure 6 indicate that there are no visible distortions in the reconstructed images. The simulation results for VLIC applied on data set-1, data set-2, data set-3, data set-4 gives an average reduction in bit rate by 85.92 %, 69.05 %, 71.44 %, 66.38 %, respectively, with SSIM nearly equal to 1. Similarly, the VOI based method applied to data set-4 gives an average

Table 3: Comparison of visually lossless bit rate (bpp), PSNR (in dB), VIF, and VSNR (in dB) of the reconstructed image for Wavelet decomposition in VLIC for levels 1–6 for data set-1 of Table1.

Label	Metric	Level-1	Level-2	Level-3	Level-4	Level-5	Level-6
CT Skull	bpp	2.156	2.064	1.928	1.747	1.54	1.52
	PSNR (dB)	52.07	51.39	51.28	51.11	50.85	50.63
	VIF	0.958	0.951	0.949	0.947	0.945	0.943
	VSNR (dB)	45.37	45.30	45.33	45.37	45.31	45.29
CT Wrist	bpp	1.29	1.231	1.040	0.914	0.807	0.803
	PSNR (dB)	54.85	53.23	52.90	52.70	52.59	52.35
	VIF	0.967	0.950	0.947	0.970	0.95	0.940
	VSNR (dB)	53.29	52.72	52.67	52.68	52.72	52.61
CT Carotid	bpp	1.744	1.656	1.427	1.218	1.160	1.158
	PSNR (dB)	54.16	52.96	52.60	52.39	52.35	52.24
	VIF	0.97	0.958	0.95	0.95	0.95	0.95
	VSNR (dB)	50.24	50.06	49.96	49.94	49.94	49.92
CT Aperts	bpp	1.173	1.190	1.032	0.833	0.715	0.708
	PSNR (dB)	57.43	56.30	55.70	55.13	54.94	54.77
	VIF	0.978	0.970	0.966	0.960	0.959	0.957
	VSNR (dB)	56.57	56.39	56.13	56.11	56.10	56.05
MRI Liver T1	bpp	2.234	2.293	1.981	0.657	1.389	1.277
	PSNR (dB)	51.63	50.57	50.12	49.82	49.66	49.54
	VIF	0.96	0.95	0.945	0.94	0.94	0.939
	VSNR (dB)	45.90	45.59	45.42	45.37	45.38	45.38
MRI Liver T2	bpp	1.744	1.585	1.400	1.270	1.208	1.199
	PSNR (dB)	52.83	52.15	51.95	51.86	51.82	51.66
	VIF	0.965	0.96	0.958	0.958	0.958	0.958
	VSNR (dB)	46.73	46.58	46.36	56.37	46.34	46.29
MRI Sag head	bpp	2.187	2.259	2.092	1.829	1.440	1.435
	PSNR (dB)	52.59	52.21	51.85	51.48	51.16	51.02
	VIF	0.95	0.944	0.94	0.93	0.93	0.93
	VSNR (dB)	52.72	52.59	52.54	52.43	52.41	52.25
MRI Ped chest	bpp	1.873	1.887	1.677	1.411	1.123	1.117
	PSNR (dB)	52.12	51.13	50.74	50.33	50.33	49.98
	VIF	0.949	0.938	0.928	0.919	0.913	0.908
	VSNR (dB)	55.65	55.55	55.42	55.34	55.30	55.28

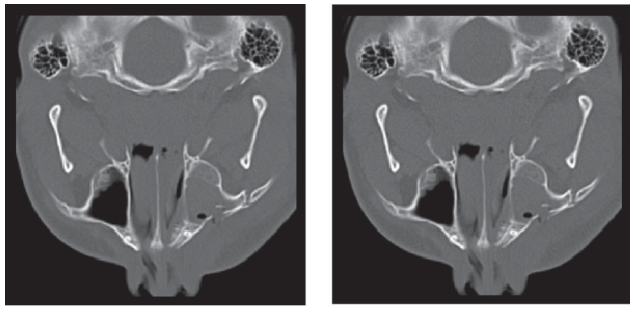

(a) (b)

Figure 3: CT skull image from data set-1 of Table 1 (a) Original Image (b) Image reconstructed with VLIC method.

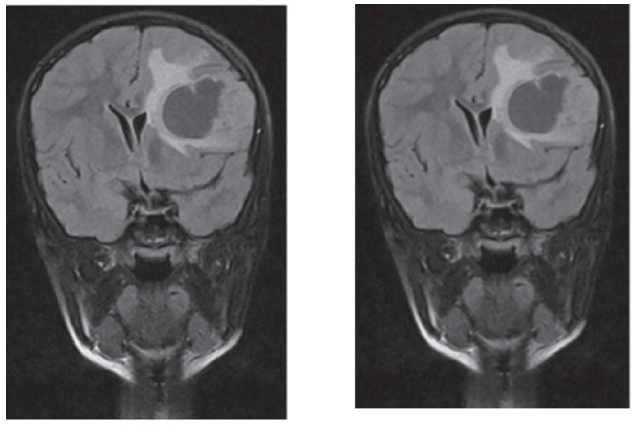

(a) (b)

Figure 4: Coronal view of MRI brain image (volume 4) from data set-4 in Table 1 (a) Original image (b) Image Reconstructed with VOI coder.

reduction in bit rate by 79.98 % for both region-A and region-B.

5.4 Performance Comparison

The method proposed in this work is visually lossless compression technique that is expected to perform better in terms of compression when compared with a lossless coder and is expected to perform better in terms of quality when compared with lossy coders. Hence, we compared our work with some of the state-of-the-art lossless coders with bit rate as the parameter and also compared with some of the lossy techniques with PSNR as the parameter. For both the above comparisons, we have considered reconstructed images with very high quality without any perceptional distortion. However,

visually lossless methods for volumetric medical images based on JND models were not found in the literature for comparison.

5.4.1 Comparison of VLIC with Lossless Compression Techniques

VLIC is compared with state-of-the-art codecs such as JPEG-LS [30], JPEG2K [31], JPEG3D [32], and MILC [33] for data set-1. For data set-2, VLIC is compared with JPEG-LS, JPEG2K, DPCM, and HEVC results obtained from [16]. For data set -3, VLIC is compared with JPEG-LS, JPEG2K, JPEG3D, and HEVC results obtained from [17]. JPEG-LS is a near-lossless/lossless compression standard. It is developed for natural images and is developed based on the prediction technique, residual modelling, and context-based coding of the residuals.

Table 4: Bit rate and quality metrics of the reconstructed image with VLIC and VOI based algorithm for data set-4 of Table 1; Region-A is VOI, Region-B is Non-VOI.

	VLIC					VOI based algorithm								
		PSNR			VSNR		PSNR (dB) for region		VIF for region		SSIM for region		VSNR (dB) for region	
Image	bpp	(dB)	VIF	SSIM	(dB)	bpp	A	B	A	B	A	B	A	B
Volume-1	4.312	74.57	0.9945	0.9997	59.68	2.974	75.25	52.82	0.9998	0.9438	0.9963	0.7575	61.79	42.87
Volume-2	4.671	73.12	0.9943	0.9998	60.45	2.466	75.26	59.95	0.9997	0.9584	0.9961	0.7729	55.88	41.26
Volume-3	3.837	74.16	0.9969	0.9996	56.41	1.973	75.27	59.96	0.9996	0.9424	0.9957	0.7537	64.56	44.26
Volume-4	3.589	74.33	0.9975	0.9995	62.53	2.022	75.27	60.88	0.9995	0.9519	0.9960	0.7739	65.43	48.81
Volume-5	3.763	74.19	0.9982	0.9995	57.98	2.575	75.26	61.07	0.9995	0.9443	0.9958	0.7501	62.32	45.54

Table 5: Comparison of VLIC bit rates with that of lossless JPEG-2K, JPEG-LS, JPEG-3D, HEVC, DPCM, and MILC coders.

Data set-1 [4]

	Visually lossless compression				Lossless compression			
	VLIC				JPEG-LS	JPEG2K	JPEG-3D	MILC
Label	PSNR (dB)	VIF	SSIM	bpp	bpp	bpp	bpp	bpp
CT Skull	50	0.945	0.997	1.42	2.728	2.955	2.120	2.030
CT Wrist	49.98	0.941	0.993	0.73	1.607	1.897	1.258	1.066
CT Carotid	49.73	0.95	0.987	1.12	1.756	2.366	1.567	1.358
CT Aperts	50.51	0.959	0.997	0.715	1.044	1.245	0.969	0.819
MRI Liver T1	49.66	0.94	0.989	1.29	3.167	3.254	2.379	2.196
MRI Liver T2	51.82	0.958	0.99	1.17	2.388	2.541	1.778	1.759
MRI Sag head	51.16	0.93	0.988	1.44	2.551	3.952	2.188	2.097
MRI Ped chest	51.59	0.913	0.992	1.12	2.901	2.985	2.131	1.655

Data set-2 [16]

	Visually lossless compression				Lossless compression			
	VLIC [35]				JPEG-LS	JPEG2K	JPEG-3D	MILC
Label	PSNR (dB)	VIF	SSIM	bpp	bpp	bpp	bpp	bpp
X-ray Angio-1	72.90	0.98	0.99	4.17	4.74	4.78	5.10	5.30
X-ray Angio-2	72.92	0.98	0.99	4.66	4.78	4.81	5.17	5.38
X-ray Angio-3	72.60	0.98	0.99	4.27	5.08	5.12	5.55	5.60
CT-1 Human Thorax	73.05	0.98	0.99	3.96	4.65	4.66	4.95	5.28
CT-2 Human Thorax	73.10	0.98	0.99	3.92	4.52	4.42	4.93	5.38
CT-3 Human Thorax	73.07	0.98	0.99	3.89	4.00	3.98	4.18	4.51
MRI Brain	50.00	0.97	0.99	2.75	3.30	3.46	3.29	3.44
MRI Cord	50.02	0.97	0.99	2.55	2.84	2.78	3.11	3.58
MRI Knee	53.9	0.98	0.99	1.26	1.48	1.59	1.55	1.62

Data set-3 [17]

	Visually lossless compression				Lossless compression			
	VLIC				JPEG-LS	JPEG2K	JPEG-3D	MILC
Label	PSNR (dB)	VIF	SSIM	bpp	bpp	bpp	bpp	bpp
CT-4 Lung scan	75.52	0.933	0.999	3.16	5.42	5.52	4.80	5.55
CT-5 Lung scan	76.7	0.943	0.997	5.86	7.83	7.93	7.45	7.93
CT-6 Spiral Arterial scan	77.01	0.984	0.998	4.40	5.89	5.87	5.20	6.14
CT-7 Female cadaver	77.48	0.956	0.997	2.25	4.01	4.09	3.85	4.28
CT-8 Human cadaver	76.04	0.923	0.999	1.70	2.99	3.20	2.84	3.07
CT-9 Chest	73.79	0.920	0.996	3.58	4.91	5.17	5.00	5.12
MRI-1 Brain	72.58	0.941	0.999	2.00	3.73	3.89	3.56	3.71
MRI-2 Brain	72.45	0.950	0.997	3.73	4.58	4.72	4.12	4.68
MRI-3 Brain	73.03	0.961	0.998	4.19	6.53	6.69	6.63	6.50

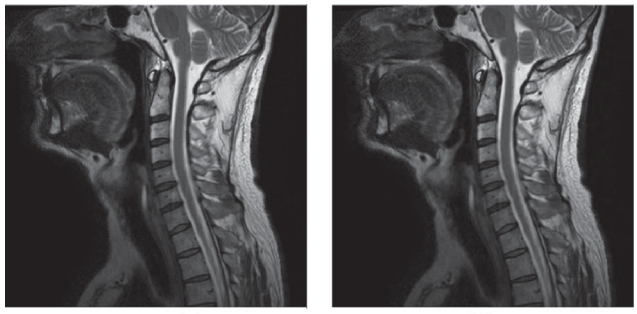

Figure 5: MRI Cord image from data set-2 of Table 1 (a) Original Image (b) Image reconstructed with VLIC method [35].

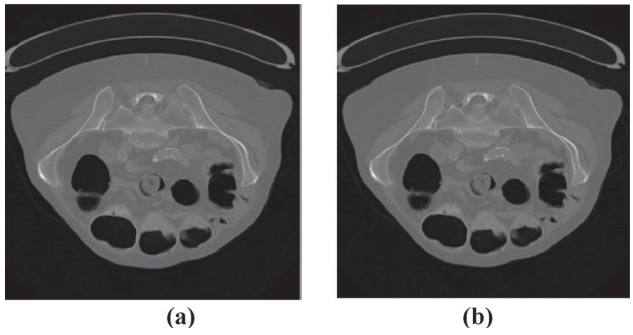

Figure 6: CT-6 Spiral Arterial scan image from data set-3 of Table 1 (a) Original Image (b) Image reconstructed with VLIC method [35].

Table 6: Comparison of VLIC bit rates (bpp) with that of HEVC [17] for data set-3 of Table 1. HEVC-All Intra(AI) mode.

	VLIC		HEVC-AII	
Image	bpp	PSNR (dB)	bpp	PSNR (dB)
CT-4	2.12	66.99	2.43	63.35
CT-5	2.97	54.70	3.00	53.07
CT-6	1.56	57.31	1.5	58.54
CT-8	1.0	67.77	1.01	66.16
CT-9	2.0	60.73	2.0	59.98
MRI-1 Brain	2.0	72.58	2.03	65.76

Table 7: Comparison of VLIC bit rates (bpp) with bit rates of JPEG2K-P1, JPEG2K-P2, and JPEG-3D [17] for data set-3 of Table 1. PSNR value is given in Db.

	VLIC			JPEG2K-P1	JPEG2K-P2	JPEG2K-3D
Image	bpp	PSNR	bpp	PSNR	PSNR	PSNR
CT-4	2.92	72.95	3.00	67.68	70.78	70.89
CT-5	2.97	54.70	3.00	54.01	55.08	55.22
CT-6	3.01	68.47	3.00	66.10	67.86	68.01
CT-7	2.25	77.48	3.00	75.49	76.73	76.84
CT-8	1.54	75.14	1.50	71.67	73.97	74.09
CT-9	2.95	68.81	3.00	67.59	68.22	68.41
MRI-1 Brain	1.38	67.25	1.50	63.09	66.02	66.13

Digital Imaging and Communications in Medicine (DICOM) standard employs JPEG2K compression technique. The 2D integer wavelet transform is used to implement the JPEG2K compression technique. HEVC is a new standard for the compression of video, that employs multi frame motion compensation and estimation. MILC is a low-complexity compression algorithm developed for 3D medical images that exploit redundancies present in 3D space using 3D linear prediction and arithmetic coding.

Comparison of VLIC and lossless compression algorithms for the test medical image data sets are tabulated in Table 5. Visually lossless bit rates given in Table 5 for all data sets are obtained by setting the value of k to 3 (Refer

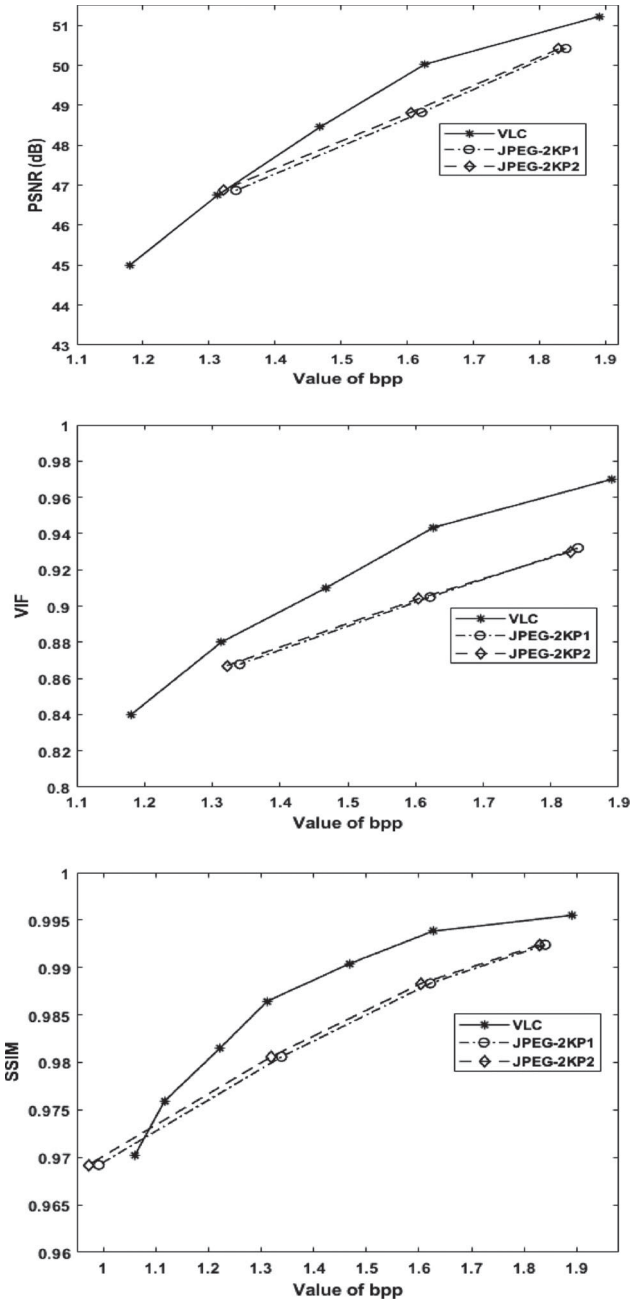

Figure 7: Comparison of PSNR, VIF, and SSIM as a function of bit rate (bpp) for VLIC with JPEG 2000 Part 1 (JPEG-2KP1) and JPEG 2000 Part 2 (JPEG-2KP2). CT Skull image from Data set-1.

Table 8: Objective and subjective evaluation of VLIC and VOI technique; Score allotted: Excellent-5; Very good-4; Good-3; Average-2; Poor-1.

	Average	Objective measure			Score	
Image	bpp	PSNR (dB)	VIF	SSIM	Radiologist	Radiographer
VLIC algorithm						
CT Skull	1.42	50	0.945	0.997	5	5
CT Wrist	0.73	49.98	0.941	0.993	5	5
MRI Liver T1	1.29	49.66	0.94	0.989	5	5
X-ray angio-1	4.17	72.90	0.98	0.99	5	5
CT-1	3.96	73.05	0.98	0.991	5	5
MRI Cord	2.55	50.02	0.97	0.99	5	5
VOI algorithm (Region A)						
Volume-1	2.974	75.25	0.99	0.99	5	5
Volume-2	2.466	75.26	0.99	0.996	5	5
Volume-3	1.973	75.27	0.99	0.995	5	5
Volume-4	2.022	75.27	0.99	0.996	5	5
Volume-5	2.575	75.26	0.99	0.995	5	5

equation 7). It is observed that for data set-1,VLIC performs better than JPEG-LS, JPEG2K, JPEG3D, and MILC in terms of compression by 48.17 %, 60.07 %, 36.41 %, 28.76 %, respectively. For data set-2 VLIC performs better than JPEG-LS, JPEG2K, DPCM, and HEVC in terms of compression by 13.28 %, 14.6 %, 20.66 %, 28.24 %, respectively. Similarly, for data set-3, VLIC performs better than JPEG-LS, JPEG2K, JPEG3D, and HEVC in terms of compression by 35.8 %, 35.93 %, 30.11 %, 35.72 %, respectively. For all these comparisons, very high quality of PSNR, VIF, and SSIM have been observed that implies that the quality of the reconstructed data is almost the same as the original image.

5.4.2 Comparison with Lossy Techniques

In this, we compare our results with some of the lossy coders as given in [17] for data set-3. Rate-distortion performance of VLIC for data set-1 is compared with JPEG-2K Part 1 and JPEG-2K Part 2 implemented using Kakadu 7.4 software [34]. In VLIC, bit rates were varied by increasing the value of k in Equation 7. PSNR obtained at a specified bit rate is compared with that obtained with lossy coders as tabulated in Tables 6 and 7 for data set-3. The plot of quality metrics PSNR, SSIM, and VIF obtained with VLIC algorithm at various bit rates shown in Figure 7 indicates that proposed coder achieves better quality for a reasonable range of bit rates.

5.4.3 Subjective Evaluation

In addition to objective assessment, the subjective evaluation was also conducted to guarantee the visual quality of the reconstructed data. For subjective evaluation, a team of six observers from the medical field comprising of radiologists and radiographers was chosen. The team was asked to rate the quality of the reconstructed image in comparison with the original image on a scale of 1–5, wherein a score of 1 represents poor, and 5 represents excellent. The objective quality and the subjective score at the specified average bit rate for the data sets are listed in Table 8. All the six radiologists have rated the reconstructed images with a rating of 5 and assessed that the coder preserved all diagnostically significant information in the brain MRI images used.

6. CONCLUSION

In this paper, we have proposed wavelet based visually lossless medical image coder for volumetric data sets. It incorporates a wavelet based vision model to identify visually irrelevant information. Important visual features such as contrast sensitivity, luminance masking, and contrast masking are modelled to determine the JND threshold. JND dependent quantizer is used to eliminate them. Inter-slice block matching is applied to remove redundancy between slices. As the proposed work removes visually redundant information, the quality of the reconstructed image is measured with PSNR and HVS based quality metrics such as SSIM, VIF, and VSNR. The performance of the proposed algorithm was compared with state-of-the-art lossless compression techniques such as JPEG-LS, JPEG-2000, JPEG-3D, HEVC, DPCM and MILC with bit rate as the parameter for comparison with quality assessment of SSIM close to 1. Results demonstrate that the proposed coder performs better in terms of compression without any degradation in the visual quality of the reconstructed image. The performance of the proposed coder was also compared with lossy coders with quality as a parameter of comparison at low bit rates. The results confirm that the proposed visually lossless coder show a better rate-distortion performance than most of the lossy coders while preserving the visual quality of the images. Another hybrid coder is also implemented where diagnostically important VOI is coded using the visually lossless method, and other regions are coded by DCT based lossy method. HVS based quality metrics like VSNR, VIF, and SSIM are used to evaluate the quality of

the reconstructed images. In addition to objective assessment, subjective assessment is carried out with the help of radiologist.

ACKNOWLEDGEMENT

The authors would like to thank Prof Bilgin A., University of Arizona, USA, Dr. Victor Sanchez, University of Warwick, UK, Dr. Tim Bruylants, Vrije University Brussel, Dr Vijay Ballal, Ampalpady Scan Centre, Udupi and Dr. Mohandas S Bhavikatti, Hubli Scan Centre, Hubli for providing the medical image data sets.

ORCID

B. K. Chandrika http://orcid.org/0000-0002-7178-3079
P. Aparna http://orcid.org/0000-0002-5096-0582
S. Sumam David http://orcid.org/0000-0001-6503-2837

REFERENCES

1. A. Nosratinia, N. Mohsenian, M. Orchard, and B. Liu, "Interframe coding of magnetic resonance images," *IEEE Trans. Med. Imaging*, Vol. 15, no. 5, pp. 639–647, 1996.

2. A. Klappenecker, F. May, and T. Beth, "Lossless compression of 3D MRI and CT data," *Proc. SPIE Int. Soc. Opt. Eng.*, Vol. 3458, pp. 140–149, 1998.

3. W. Dajun, and T. Chon. "Lossless medical image compression algorithm exploring three-dimensional space," WCC 2000-ICSP 2000. *2000 5th International Conference on Signal Processing Proceedings*. 16th World Computer Congress, Vol. 2, pp. 1062–1064, IEEE, 2000.

4. A. Bilgin, G. Zweig, and M. W. Marcellin. "Efficient lossless coding of medical image volumes using reversible integer wavelet transforms," *Proceedings DCC'98 Data Compression Conference*, pp. 428–437, IEEE, 1998.

5. G. Menegaz, and J. Thiran, "Lossy to lossless object-based coding of 3-D MRI data," *IEEE Trans. Image Process.*, Vol. 11, no. 9, pp. 1053–1061, 2002.

6. G. Menegaz, and J. Thiran, "Three-dimensional encoding/two-dimensional decoding of medical data," *IEEE Trans. Med. Imaging*, Vol. 22, no. 3, pp. 424–440, 2003.

7. Z. Xiong, X. Wu, S. Cheng, and J. Hua, "Lossy-to-lossless compression of medical volumetric data using three-dimensional integer wavelet transforms," *IEEE Trans. Med. Imaging*, Vol. 22, no. 3, pp. 459–470, 2003.

8. P. E. Sophia, and J. Anitha, "A hybrid contextual compression technique using wavelet and contourlet transforms with PSO optimized prediction," *Int. J. Imaging Syst. Technol.*, Vol. 27, no. 2, pp. 171–181, 2017.

9. A. F. Guarda, J. M. Santos, L. A. da Silva Cruz, P. A. Assuncao, N. M. Rodrigues, and S. M. de Faria, "A method to improve HEVC lossless coding of volumetric medical images," *Signal Process., Image Commun.*, Vol. 59, pp. 96–104, 2017.

10. Z. Zuo, X. Lan, L. Deng, S. Yao, and X. Wang, "An improved medical image compression technique with lossless region of interest," *Optik. (Stuttg)*, Vol. 126, no. 21, pp. 2825–2831, 2015.

11. M. Kaur, and V. Wasson, "ROI based medical image compression for telemedicine application," *Procedia. Comput. Sci.*, Vol. 70, pp. 579–585, 2015.

12. H. Hamout, and A. Elyousfi. "Low complexity intra mode decision algorithm for 3D-HEVC," *25th European Signal Processing Conference* (EUSIPCO), pp. 1475–1479, IEEE, 2017.

13. D. Yee, S. Soltaninejad, D. Hazarika, G. Mbuyi, R. Barnwal, and A. Basu. "Medical image compression based on region of interest using better portable graphics (BPG)," *IEEE International Conference on Systems, Man, and Cybernetics (SMC)*, pp. 216–221, IEEE, 2017.

14. V. Sanchez, R. Abugharbieh, and P. Nasiopoulos, "3-D scalable medical image compression with optimized volume of interest coding," *IEEE Trans. Med. Imaging*, Vol. 29, no. 10, pp. 1808–1820, 2010.

15. J. Taquet, and C. Labit, "Hierarchical oriented predictions for resolution scalable lossless and near-lossless compression of CT and MRI biomedical images," *IEEE Trans. Image Process.*, Vol. 21, no. 5, pp. 2641–2652, 2012.

16. V. Sanchez, and J. Bartrina-Rapesta. "Lossless compr ession of medical images based on HEVC intra coding," *IEEE International Conference on Acoustics, Speech and Signal Processing (ICASSP)*, pp. 6622–6626, IEEE, 2014.

17. T. Bruylants, A. Munteanu, and P. Schelkens, "Wavelet based volumetric medical image compression," *Signal Process., Image Commun.*, Vol. 31, pp. 112–133, 2015.

18. D. Wu, D. Tan, M. Baird, J. DeCampo, C. White, and H. Wu, "Perceptually lossless medical image coding," *IEEE Trans. Med. Imaging*, Vol. 25, no. 3, pp. 335–344, 2006.

19. Z. Liu, L. J. Karam, and A. B. Watson, "JPEG2000 encoding with perceptual distortion control," *IEEE Trans. Image Process.*, Vol. 15, no. 7, pp. 1763–1778, 2006.

20. C. Xu, and J. L. Prince, "Snakes, shapes, and gradient vector flow," *IEEE Trans. Image Process.*, Vol. 7, no. 3, pp. 359–369, 1998.

21. K. Fukunaga. *Introduction to statistical pattern recognition*. Amsterdam: Elsevier, 2013.

22. G. K. Wallace, "The JPEG still picture compression standar," *IEEE Trans. Consum. Electron.*, Vol. 38, no. 1, pp. 18–34, 1992.

23. H. R. Sheikh, and A. C. Bovik. "Image information and visual quality," *IEEE International Conference on Acoustics, Speech, and Signal Processing*, Vol. 3, pp. 430–444, IEEE, 2004.

24. Z. Wang, A. C. Bovik, H. R. Sheikh, and E. P. Simoncelli, "Image quality assessment: from error visibility to structural similarity," *IEEE Trans. Image Process.*, Vol. 13, no. 4, pp. 600–612, 2004.

25. M. Razaak, M. G. Martini, and K. Savino, "A study on quality assessment for medical ultrasound video compressed via HEVC," *IEEE. J. Biomed. Health. Inform.*, Vol. 18, no. 5, pp. 1552–1559, 2014.

26. I. A. Kowalik-Urbaniak, J. Castelli, N. Hemmati, D. Koff, N. Smolarski-Koff, E. R. Vrscay, J. Wang, and Z. Wang, "Modelling of subjective radiological assessments with objective image quality measures of brain and body CT images," *International Conference Image Analysis and Recognition*, pp. 3–13, Springer, Cham, 2015.

27. D. M. Chandler, and S. S. Hemami, "VSNR: A wavelet-based visual signal-to-noise ratio for natural images," *IEEE Trans. Image Process.*, Vol. 16, no. 9, pp. 2284–2298, 2007.

28. I. Kowalik-Urbaniak, D. Brunet, J. Wang, D. Koff, N. Smolarski-Koff, E. R. Vrscay, B. Wallace, and Z. Wang, "The quest for diagnostically lossless medical image compression: a comparative study of objective quality metrics for compressed medical image," *International Society for Optics and Photonics*, Vol. 9037, pp. 903717–903717, 2014.

29. A. B. Watson, G. Y. Yang, J. Solomon, and J. Villasenor, "Visibility of wavelet quantization nois," *IEEE Trans. Image Process.*, Vol. 6, no. 8, pp. 1164–1175, 1997.

30. HP-LABS. LOCO-1/JPEG-LS: JPEG-LS reference encoder - V.1.00, http://www.hpl.hp.com/loco, (Accessed on January 2019).

31. OPEN-JPEG. Openjpeg, open source c-libary for jpeg 2000, https://code.google.com/p/openjpeg/wiki/Downloads?tm=2, (Accessed on January 2019).

32. OPEN-JPEG-3D. Openjpeg, open source C-library for JPEG 3D, https://code.google.com/p/openjpeg/downloads/detail?name=openjpeg3d_v1_3.tar.gz&can=4&q=, (Accessed on January 2019).

33. R. Pizzolante, and B. Carpentieri. "Lossless, low-complexity, compression of three-dimensional volumetric medical images via linear prediction," *18th International Conference on Digital Signal Processing (DSP)*, pp. 1–6, IEEE, 2013.

34. KAKADU, KAKADU Version 7.4 JPEG2000 software development tool kit, http://kakadusoftware.com/, (Accessed on January 2019).

35. B. K. Chandrika, P. Aparna, and S. Sumam David. "Irreversible wavelet compression of radiological images based on visual threshold," IEEE International WIE Conference on Electrical and Computer Engineering (WIECON-ECE). IEEE, 2015.

Authors

B K Chandrika is associate professor at Department of Electrical and Electronics Engineering, Manipal Institute of Technology, Manipal Academy of Higher Education, Manipal, India. She obtained her BTech degree in electrical and electronics engineering, MTech in industrial electronics and PhD from NITK, Surathkal. Her areas of interest are signal processing, signal compression, and FPGA based system design.

Corresponding author. Email: chandrika.bk@manipal.edu

P Aparna obtained her BTech degree in electronics & communication engineering from NMAMIT. Nitte (Mangalore University) in 1999 and her MTech degree in digital electronics & advanced communication from NITK, Surathkal in 2004 and her PhD from NITK Surathkal in multimedia signal processing in 2012. She has joined Electronics & Communication Dept, NITK, Surathkal as assistant professor in 2008. Her areas of interest are biomedical signal processing, signal compression, computer architecture and embedded systems. She has published 20 research papers in various journals and conference proceedings.

Email: p.aparnadinesh@gmail.com

S Sumam David is a professor at Department of Electronics and Communication Engineering, National Institute of Technology Karnataka, Surathkal, Mangalore, India. She obtained her BTech degree from University of Kerala, India in 1985, MTech and PhD degrees from Department of Electrical Engineering, Indian Institute of Technology, Madras, India in 1986 and 1992, respectively. She joined NITK Surathkal as faculty in August 1991. She has served as head of the Department of Electronics and Communication Engineering and dean (Academic) of the Institute. Her research interests are in the areas of signal processing, VLSI architectures for signal processing and engineering education. She is a Fellow of IETE, Fellow of IE, and Senior Member of IEEE Signal Processing Society.

Email: sumam@ieee.org